Applied Problems of Nonlinear Oscillation and Wave Theory

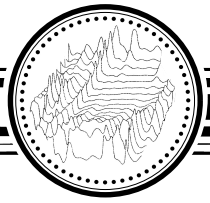

Article DOI: 10.18500/0869-6632-003203

Stability of motion and drift of a rigid body in a non-contact inductive electromagnetic suspension

P. P. Udalov[1] ✉, *A. V. Lukin*[1], *I. A. Popov*[1], *L. V. Shtukin*[1], *K. V. Poletkin*[2]

[1]Peter the Great St. Petersburg Polytechnic University, Russia
[2]Hefei University of Technology, China
E-mail: ✉udalov_pp@spbstu.ru, lukin_av@spbstu.ru, popov_ia@spbstu.ru, shtukin_lv@spbstu.ru, 022810003@hfut.edu.cn

Received 4.06.2025, accepted 27.11.2025, available online 27.11.2025, published 31.03.2026

Abstract. *Purpose* of this work is to study the nonlinear dynamics and stability of the motion of a conducting thin ring in the electromagnetic field of two circular inductors. *Methods.* The analysis is performed using asymptotic methods of nonlinear mechanics. Numerical methods of bifurcation theory are used to study the average position of a levitating body in the space of key suspension parameters over the period of a rapidly oscillating field. *Results.* Assuming a slow evolution of the average position of a levitating body, the conditions for the occurrence and parameters of drift are determined. The stability of the levitation regime is investigated in a refined asymptotic formulation. *Conclusion.* It is shown that taking into account the possibility of slow evolution of the average position of a levitating body leads to the formulation of a stability condition related to the relationship between the dissipation of mechanical and electrical nature.

Keywords: induction suspension, electromagnetic suspension, electromagnetic induction, levitation, nonlinear dynamics, stability of oscillations, method of multiple scales.

Acknowledgements. The work was supported by the Russian Science Foundation, grant no. 25-21-00402, https://rscf.ru/project/25-21-00402/

For citation: Udalov PP, Lukin AV, Popov IA, Shtukin LV, Poletkin KV. Stability of motion and drift of a rigid body in a non-contact inductive electromagnetic suspension. Izvestiya VUZ. Applied Nonlinear Dynamics. 2026;34(2):247–267. DOI: 10.18500/0869-6632-003203

Introduction

An electromagnetic suspension is an element of navigation, transportation, and electrical systems [1] that operates based on the principle of electromagnetic levitation (EL) and balances the gravity of a conducting rigid body (RB) using ponderomotive forces [2–6]. The design of EL-based devices allows for high reliability [7], stability [8], and extended uptime [9, 10]. EL-based devices have found applications in navigation instrumentation (micromechanical accelerometers [11], gyroscopes [12–15], gravimeters/seismic sensors [16]), microoptoelectromechanical systems (scanning micro mirrors) [11, 17, 18], sorting manipulators [19], magnetic levitation trains [20, 21], automotive suspension [22], wireless energy transmission systems [23], devices for measuring the magnetic properties of liquids [24] and more.

When developing a non-contact suspension as an element of micromechanical inertial sensors, the

levitation RB is usually made in the form of a simple geometric object (disk [7], ring [25], rectangular plate [26], sphere [27]) and is made of a conductive material. The alternating electromagnetic field created by the coil system [28, 29] induces eddy currents in the RB. Under certain conditions, the interaction of the induction currents with the coil currents can lead to a stable levitation regime of the RB [3]. In work [12], it is shown that in order to ensure the stability of the levitation state with respect to spatial disturbances, it is necessary to introduce an additional inductor into the device design, which is powered by a current that is in antiphase with the current of the main coil of a smaller radius.

Many works are devoted to analytical, numerical, and experimental studies of the regimes of operation and characteristics of the electromagnetic suspension. In [7, 11, 13, 14, 30], the development of an inertial sensor with a disk-shaped sensitive element based on the electromagnetic suspension is discussed. In [31, 32], an experimental prototype of an electromagnetic suspension with volumetric inductors (solenoids, spiral coils) is considered.

In works [33, 34], analytical models of an accelerometer and a gyroscope, respectively, based on the EL principle, are investigated. In [35], a linearized model of the oscillations of a levitating RB is studied. In [7, 36], the issues of choosing the optimal radii of the inductors and the disk-shaped RB are discussed.

In [37, 38], analytical calculations of the intrinsic and mutual inductances of wires and circuits are performed. In [39, 40], estimates of the forces and rigidity of the sensitive element of the induction suspension are provided. In [41], the stability of the induction suspension is investigated. The works [26, 42] are devoted to experimental and analytical studies of the collapse effect, which consists in the adhesion of the electromagnetic suspension's RB to the capacitor plates when the critical voltage is reached, both for the disk-shaped and rectangular forms in terms of inertial masses. Numerical studies of the operation regimes and force characteristics of the electromagnetic suspension device based on the finite element method are presented in [34, 43–46].

Analytical approaches to the study of the dynamics of the electromagnetic suspension of the RB [26, 33, 34, 42] are based on the key assumption of the constant levitating height. This assumption allows us to linearize the system in the vicinity of the equilibrium position and obtain the stability conditions for the conservative model. However, as the numerical analysis of the full nonlinear model shows, this assumption is limited, and there is an unstable region of the suspension for small levitating heights. In order to account for the significant feature of the body motion in the suspension (in reality, the averaged levitating height over a rapidly oscillating field is a slow function of time), this paper develops an approach with explicit modeling of the dependence of the levitating height on the slow time, which constitutes the main scientific novelty of the study.

The main goal of this work is to analytically study the dynamics of a ring-shaped RB in the field of two circular inductors, assuming that the levitation height is a slowly changing function of time, that is, it drifts near its average position.

The work is structured as follows: Section 1 presents the construction of an analytical model of RB vertical oscillations, Section 2 provides an asymptotic analysis of the dynamics of the original system using the method of multiple scales, Section 3 presents the results of the study, and Section Conclusion provides general conclusions about the work.

1. Mathematical model

The article considers a model of vertical movements of the RB of a non-contact inductive suspension made in the form of a thin, non-deformable rectangular ring in an alternating electromagnetic field of two circular inductors. A schematic representation of the device is shown in Fig. 1. A three-dimensional model of a possible design of an electromagnetic suspension is presented in Fig. 2.

When an alternating current $i_l = I_l \sin \omega t$ (I_l and ω are the amplitude and frequency of the current i_l) is applied to the levitation inductor of average radius r_l and thickness t_l (Fig. 1 shows it as number 3) , an alternating electromagnetic field is generated that interacts with the field of eddy currents in the RB volume, which is shaped like a square-section ring of average radius r_{pm} and thickness t_{pm} (Fig. 1 shows it as number 1). The Ampere force between the current i_l and the induced current i_{pm} can, under certain conditions, lead to RB levitation (compensate for gravity and ensure stable motion). The stabilizing inductor, which carries the current $i_s = I_s \sin \omega t$ (I_s and ω are the amplitude and frequency

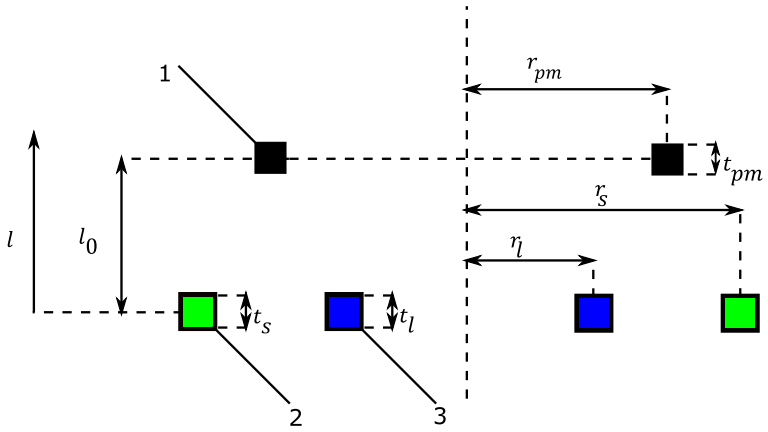

Fig. 1. Schematic view of inductive non-contact suspension; 1 — rigid body (RB), 2 and 3 — stabilizing and levitation coils, respectively (color online)

of the current i_s), shown as number 2 in Fig. 1, prevents lateral and angular displacements of the RB and ensures spatial stability. The resulting electromagnetic field is a superposition of the electromagnetic fields generated by the levitation and stabilizing inductions. The parameter I_s can take both positive and negative values: $I_s/I_l = 1$ corresponds to the case of in phase currents i_l and i_s, $I_s/I_l = -1$ corresponds to out of phase currents, and, $I_s/I_l = 0$ corresponds to the absence of current in the stabilizing inductor. Changing the value of I_s changes both the amplitude and the direction of the current i_s.

The system of RB oscillation equations in dimensionless form is written as follows [47]:

$$\xi_l'' + \varepsilon^2\lambda\xi_l' = \varepsilon^2\left(\alpha m^{\xi_l} j_{pm}\sin\tau - 1\right), \quad j_{pm}' + r j_{pm} = -m\cos\tau - m^{\xi_l}\xi_l'\sin\tau, \tag{1}$$

where

$$\xi_l = \frac{l}{r_l},\ \xi_{l0} = \frac{l_0}{r_l},\ j_s = \frac{I_s}{I_l},\ j_{pm} = \frac{i_{pm}}{I_l},\ \tau = \omega t,\ \varepsilon^2 = \frac{g}{\omega^2 r_l},\ \alpha = \frac{L_{pm}I_l^2}{\hat{m}g r_l},\ r = \frac{R_{pm}}{L_{pm}\omega},$$

$$\lambda = \frac{\lambda_l}{\hat{m}\omega}, \quad b_l = \frac{r_{pm}}{r_l}, \quad b_s = \frac{r_{pm}}{r_s}, \quad \hat{\kappa}_l^2 = \frac{4b_l}{(1+b_l)^2 + \xi_l^2}, \quad \hat{\kappa}_s^2 = \frac{4b_s}{(1+b_s)^2 + (\frac{b_s}{b_l})^2\xi_l^2},$$

$$m_{l,s|pm} = \frac{M_{l,s|pm}}{L_{pm}} = \frac{w_{l,s}}{\hat{L}}\frac{\Phi(\hat{\kappa}_{l,s})}{\sqrt{b_{l,s}}}, \quad \Phi(\hat{\kappa}_{l,s}) = \left(\frac{2}{\hat{\kappa}_{l,s}} - \hat{\kappa}_{l,s}\right)K(\hat{\kappa}_{l,s}^2) - \frac{2}{\hat{\kappa}_{l,s}}E(\hat{\kappa}_{l,s}^2), \tag{2}$$

$$m = m_{l|pm} + j_s m_{s|pm}, \quad \hat{L} = \ln(\frac{8r_{pm}}{S_{pm}}) - 2,$$

$$S_{pm} = \exp\left(\ln t_{pm} + \frac{1}{3}(\ln 2 + \pi) - \frac{25}{12}\right) \approx 0.44705 t_{pm},$$

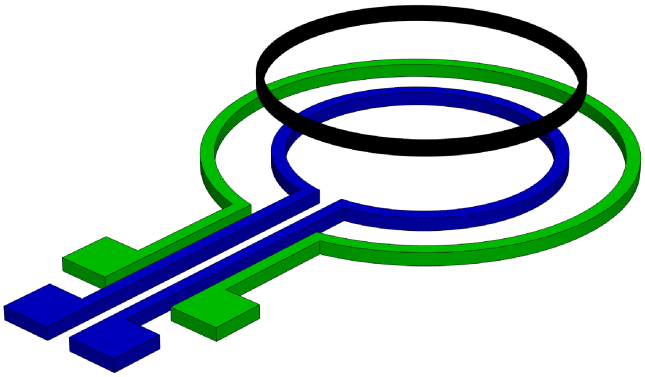

Fig. 2. Three-dimensional model of inductive non-contact suspension (color online)

t is the time, g is the acceleration of free fall, $\hat{m}$ is the mass of the RB, R_{pm} is the electrical resistance of the RB, λ_l is the coefficient of viscous energy dissipation into the environment, $L_{pm} = \mu_0 r_{pm} \hat{L}$ is the intrinsic inductance of the RB, $M_{l|pm}$ is the mutual inductance between the levitation coil and the RB, $M_{s|pm}$ is the mutual inductance between the stabilization coil and the RB, $\hat{\kappa}_{l,s}$ are the elliptic modules; $K(\hat{\kappa}^2_{l,s})$, $E(\hat{\kappa}^2_{l,s})$ are the complete elliptic integrals of the first and second kinds, respectively, $\hat{\kappa}_{l,s}$ are the elliptic modules, $(\quad)' = \frac{\partial}{\partial \tau}$, $(\quad)^{\xi_l} = \frac{\partial}{\partial \xi_l}$, l is the vertical displacement of the RB, l_0 is the characteristic scale of the vertical displacement, which is taken to be equal to the coordinate of the middle position of the RB; $w_{l,s}$ is the number of turns in the levitation and stabilization coils, and S_{pm} is the average geometric cross-section of the RB [37, 38].

It should be noted that the right-hand sides of system (1) depend nonlinearly on the unknown variables ξ_l and j_{pm} due to the presence of terms containing mutual inductance and its derivatives.

When choosing the operating regime of the suspension, it is important to ensure that the fast electrical and slow mechanical motions are separated. In this case, the parameter ε, which represents the ratio of the squares of the characteristic frequencies of the mechanical and electrical nature, is small. This feature of the basic system of equations allows the use of asymptotic methods of nonlinear mechanics for constructing approximate solutions and analyzing stability.

2. Construction of an asymptotic solution

To find a uniformly suitable solution to system (1) , we use the method of multiple scales [48]. To do this, we represent the desired functions as the following expansions in a small parameter ε:

$$\begin{gathered} j_{pm}(\varepsilon, T_0, T_1, T_2) = j_0(T_0, T_1, T_2) + \varepsilon j_1(T_0, T_1, T_2) + \varepsilon^2 j_2(T_0, T_1, T_2), \\ \xi_l(\varepsilon, T_0, T_1, T_2) = \xi_{l0}(T_1, T_2) + \varepsilon \xi_{l1}(T_0, T_1, T_2) + \varepsilon^2 \xi_{l2}(T_0, T_1, T_2), \\ m(\varepsilon, T_0, T_1, T_2) = m_0 + m_l(\xi_l - \xi_{l0}) + \frac{1}{2} m_{ll}(\xi_l - \xi_{l0})^2, \\ \frac{\partial}{\partial \tau} = D_0 + \varepsilon D_1 + \varepsilon^2 D_2, \quad \frac{\partial^2}{\partial \tau^2} = D_0^2 + 2\varepsilon D_0 D_1 + \varepsilon^2 \left(D_1^2 + 2 D_0 D_2\right), \end{gathered} \tag{3}$$

where $T_n = \varepsilon^n \tau$, $D_n = \frac{\partial}{\partial T_n}$, $m_0 = m(\xi_{l0})$, $m_l = m^{\xi_l}(\xi_{l0})$, $m_{ll} = m^{\xi_l \xi_l}(\xi_{l0})$.

Substituting (3) into (1) and equating the coefficients with the same powers of ε, we obtain $\underline{\varepsilon^0}$

$$D_0 j_0 + r j_0 = -m_l D_0 \xi_{l0} \sin T_0 - m_0 \cos T_0, \quad D_0^2 \xi_{l0} = 0, \tag{4}$$

$\underline{\varepsilon^1}$

$$\begin{gathered} D_0 j_1 + r j_1 = -D_1 j_0 - \xi_{l1} m_l \cos T_0 - \left(m_l \left(D_0 \xi_{l1} + D_1 \xi_{l0}\right) + m_{ll} \xi_{l1} D_0 \xi_{l0}\right) \sin T_0, \\ D_0^2 \xi_{l1} = -2 D_0 D_1 \xi_{l0}, \end{gathered} \tag{5}$$

$\underline{\varepsilon^2}$

$$\begin{gathered} D_0 j_2 + r j_2 = -D_1 j_1 - D_2 j_0 - \left(m_l \xi_{l2} + \frac{m_{ll} \xi_{l1}^2}{2}\right) \cos T_0 - \\ - \left(\left(D_0 \xi_{l2} + D_1 \xi_{l1} + D_2 \xi_{l0}\right) m_l + \left(\xi_{l2} D_0 \xi_{l0} + \left(D_0 \xi_{l1} + D_1 \xi_{l0}\right) \xi_{l1}\right) m_{ll}\right) \sin T_0, \\ D_0^2 \xi_{l2} = -2 D_0 D_1 \xi_{l1} - 2 D_0 D_2 \xi_{l0} - D_1^2 \xi_{l0} - \lambda D_0 \xi_{l0} + \alpha m_l j_0 \sin T_0 - 1, \end{gathered} \tag{6}$$

$\underline{\varepsilon^3}$

$$\begin{gathered} D_0 j_3 + r j_3 = -D_1 j_2 - D_2 j_1 - (m_l (D_2 \xi_{l1} + D_1 \xi_{l2} + D_0 \xi_{l3}) + \\ + m_{ll} \xi_{l1} (D_2 \xi_{l0} + D_1 \xi_{l1} + D_0 \xi_{l2}) + D_0 \xi_{l0} m_{ll} \xi_{l3} + \\ + m_{ll} \xi_{l2} (D_1 \xi_{l0} + D_0 \xi_{l1})) \sin T_0 - (m_l \xi_{l3} + m_{ll} \xi_{l1} \xi_{l2}) \cos T_0, \\ D_0^2 \xi_{l3} = -2 D_0 D_1 \xi_{l2} - 2 D_0 D_2 \xi_{l1} - D_1^2 \xi_{l1} - 2 D_1 D_2 \xi_{l0} - \\ - \lambda (D_0 \xi_{l1} + D_1 \xi_{l0}) - \alpha (m_l j_1 + m_{ll} \xi_{l1} j_0) \sin T_0. \end{gathered} \tag{7}$$

The partial solution of equation (4) can be represented as

$$\xi_{l0} = \xi_{l0}(T_1, T_2), \quad j_0 = -m_0 \cos\gamma \sin(T_0 + \gamma), \tag{8}$$

where $\tan\gamma = r$.

Note that the expression for ξ_{l0} does not include a linearly growing, obviously secular term of the general solution of the homogeneous equation; the expression for the current j_0 also does not include the aperiodic transition term in the solution.

The solution of system (5) is written as

$$\xi_{l1} = 0, \quad j_1 = \frac{1 - \cos 4\gamma}{4} m_l D_1 \xi_{l0} \cos T_0 + \frac{\sin 4\gamma}{4} m_l D_1 \xi_{l0} \sin T_0. \tag{9}$$

Taking into account (9), the second equation in (6) is written as

$$D_0^2 \xi_{l2} = -D_1^2 \xi_{l0} - \frac{\alpha \cos^2\gamma}{2} m_0 m_l - 1 + \frac{\alpha \cos\gamma}{2} m_0 m_l \cos(2T_0 + \gamma). \tag{10}$$

In order to get rid of the secular terms in the equation for ξ_{l2}, let us put

$$D_1^2 \xi_{l0} = -\frac{\alpha \cos^2\gamma}{2} m_0(\xi_{l0}) m_l(\xi_{l0}) - 1, \tag{11}$$

where from

$$\xi_{l2} = -\frac{\alpha \cos\gamma}{8} m_0 m_l \cos(2T_0 + \gamma). \tag{12}$$

Equation (11) defines the slow evolution of the levitation height ξ_{l0}.

Multiply (11) by the value $d\xi_{l0}$, integrate the displacement ξ_{l0} in the range $[\xi_{st} \quad \xi_{l0}]$, and obtain

$$dT_1 = \pm \frac{1}{\sqrt{2}} \frac{d\xi_{l0}}{\sqrt{h(T_2) + h_0 - \xi_{l0} - \frac{\alpha \cos^2\gamma}{4} m_0^2}}, \tag{13}$$

where $h_0 = \xi_{st} + \frac{\alpha \cos^2\gamma}{4} m_0^2(\xi_{st})$, $h(T_2)$ is an integration constant, and ξ_{st} is the equilibrium position of the dynamic system, which is determined by setting the right-hand side of the equation to zero (11):

$$\frac{\alpha \cos^2\gamma}{2} m_0(\xi_{st}) m_l(\xi_{st}) + 1 = 0. \tag{14}$$

The stability of the equilibrium position ξ_{st} is determined by

$$\frac{\partial}{\partial \xi_{l0}} \left(m_0(\xi_{st}) m_l(\xi_{st}) + \frac{2}{\alpha \cos^2\gamma} \right) > 0 \Rightarrow m_l^2(\xi_{st}) + m_0(\xi_{st}) m_{ll}(\xi_{st}) > 0, \tag{15}$$

which agrees with the results obtained from studying small oscillations of the electromagnetic suspension near the average position of the RB ξ_{st} [35].

Assuming that the RB oscillates near its average position ξ_{st}, we expand the radical in a Taylor series and rewrite (13) as

$$dT_1 = \pm \frac{1}{\sqrt{2}} \frac{dy}{\sqrt{h(T_2) - by^2}}, \tag{16}$$

where $y = \xi_{l0} - \xi_{st}$, $b = \frac{\alpha \cos^2\gamma}{4} \left(m_0(\xi_{st}) m_{ll}(\xi_{st}) + m_l^2(\xi_{st}) \right)$.

Equation (16) gives a quadrature solution for the oscillations of an equivalent linear oscillator. After integrating the left and right sides of (16), we obtain

$$T_1 = \frac{1}{\sqrt{2}} \frac{1}{\sqrt{b}} \arcsin \sqrt{\frac{b}{h(T_2)}} (\xi_{l0} - \xi_{st}), \tag{17}$$

from which

$$\xi_{l0} = \xi_{st} + \sqrt{\frac{h(T_2)}{b}} \sin \sqrt{2b} T_1. \tag{18}$$

Solution (18) indicates the fact of slow oscillations (drift) of the levitation height ξ_{l0} near the equilibrium position ξ_{st} with an amplitude of $\sqrt{\frac{h}{b}}$ and a frequency of $\sqrt{2b}$.

Substituting (8), (9), (12) into the second equation in (7), we obtain

$$D_0^2\xi_{l3} = -2D_1D_2\xi_{l0} - \left(\lambda - \frac{\alpha\sin 4\gamma}{8}m_l^2\right)D_1\xi_{l0}+\text{n.s.t.}, \tag{19}$$

where n.s.t. stands for non-secular terms [48].

The condition for the absence of secular terms in (19) leads to the following relationship

$$D_1D_2\xi_{l0} = -\frac{1}{2}\left(\lambda - \frac{\alpha\sin 4\gamma}{8}m_l^2\right)D_1\xi_{l0}. \tag{20}$$

After substituting (18) into (19), we obtain

$$D_2\sqrt{h} = -\frac{1}{2}\left(\lambda - \frac{\alpha\sin 4\gamma}{8}m_l^2\right)\sqrt{h}. \tag{21}$$

Equation (21) describes the slow change of the total mechanical energy of the nonlinear oscillator (11), measured from the minimum of its potential energy.

The equilibrium state h^* (21) is determined from the equality of its right-hand side to zero:

$$h^* = 0, \tag{22}$$

which corresponds to $\xi_{l0} = \xi_{st}$.

The stability of the equilibrium state h^* is determined by

$$\lambda - \frac{\alpha\sin 4\gamma}{8}m_l^2(\xi_{st}) > 0 \tag{23}$$

or, taking into account (14)

$$\lambda + \cos 2\gamma\tan\gamma\frac{m_l(\xi_{st})}{m_0(\xi_{st})} > 0. \tag{24}$$

Inequality (24) defines the regions in the parameter space of the system in which total mechanical energy (21) h does not increase with time. It can be seen that condition (24) expresses the relationship between the mechanical λ and electrical $\cos 2\gamma\tan\gamma\frac{m_l(\xi_{st})}{m_0(\xi_{st})}$ dissipation, the sign of which determines the stability of the RB levitating motion.

Thus, the asymptotic approximation of the solution to the initial problem (1) takes the form

$$\xi_l = \xi_{st} + \sqrt{\frac{h(\varepsilon^2\tau)}{b}}\sin\sqrt{2b}\varepsilon\tau + \frac{\varepsilon^2}{4\cos\gamma}\cos(2\tau+\gamma), \quad j_{pm} = -m_0\cos\gamma\sin(\tau+\gamma), \tag{25}$$

where $h(\varepsilon^2\tau)$ is determined from solution (21).

The steady state solution, when condition (24) of no drift of the RB average position is satisfied, has the form

$$\xi_l = \xi_{st} + \frac{\varepsilon^2}{4\cos\gamma}\cos(2\tau+\gamma), \quad j_{pm} = -m_0(\xi_{st})\cos\gamma\sin(\tau+\gamma), \tag{26}$$

where the relationship between α and ξ_{st} is taken into account according to (14). The stability of ξ_{st} is determined from (15).

3. Results

Next, we compare the analytical results according to (26) with the data from a numerical calculation performed in the Matlab software package (system (1) was integrated using the built-in ode45 function with the initial conditions $[\xi_l, \xi_l', j_{pm}]_{\tau=0} = [0.4, 0, 0]$ [49]). The parameters used for the calculation are listed in Table 1.

Table 1. System's parameters

Parameter	λ	ε	b_l	α	γ	w_l	w_s	r_l	r_s	t_{pm}	j_s
Value	10	0.01	1.2	0.2534	0.61	14	12	1 mm	1.9 mm	0.1 mm	−0.5

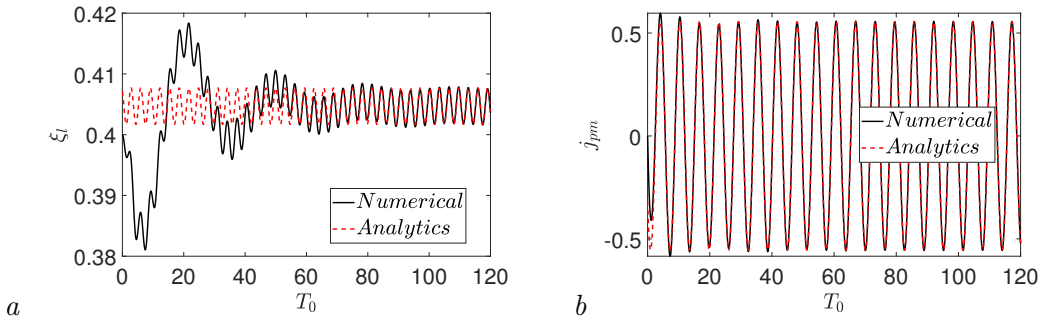

Fig. 3. Graph comparing dimensionless value of a — RB displacement, b — induced current from dimensionless time T_0 in case of direct numerical calculation (black solid lines) and analytical equations (26) (dotted red line) (color online)

Fig. 3 shows the graph comparison of the RB oscillations and induced current in the case of numerical calculation and analytical expressions (26).

Fig. 3 shows that the analytical solution (26) coincides with the numerical results to a sufficient degree of accuracy in the case of steady state RB oscillations.

To study the bifurcations of the equilibrium states of dynamic system (11) depending on the system parameters, the MatCont software package of numerical algorithms for bifurcation theory is used [50]. Fig. 4, a – 6, a show the dependence of the average position of the RB ξ_{l0} on the parameters α, j_s, γ. The solid lines represent stable equilibrium positions, while the dotted lines represent unstable equilibrium positions. The pink circles indicate the bifurcation points, which separate the region of no equilibrium states in the parameter space from the region of two (or one in the case of bifurcation) non-trivial equilibrium positions. The calculated and averaged values of the levitation height of system (1) using the ode45 function are denoted by square symbols. Fig. 4, b – 6, b show the characteristic zones where an equilibrium position exists (II) / or does not exist (I) depending on the system parameters.

Fig. 4, a, b shows the dependence of the average position of RB ξ_{l0} on the parameter α, which is directly proportional to the square of the amplitude of the current of the levitation coil I_l, when the parameter j_s is varied. It can be seen that there are «critical» values of the parameter $\alpha = \alpha_{crit}$ (the

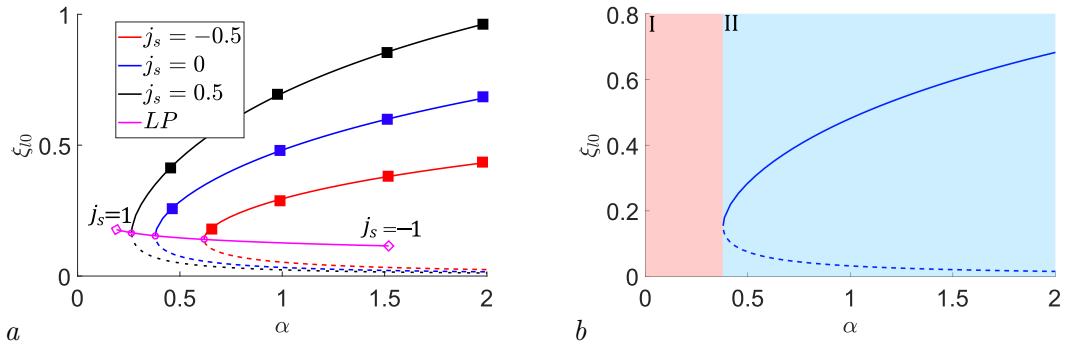

Fig. 4. a — Dependence of the average position of RB ξ_{l0} on the parameter α at $j_s = -0.5, 0, 0.5$ (red, blue, black lines, respectively); the pink line (LP) indicates the zone of separation of stable (solid lines) and unstable (dashed lines) branches when varying the parameter $j_s = [-1; 1]$; b — depiction of characteristic zones of existence and nonexistence of equilibrium positions at j_s=0, $\varepsilon = 0.001$, $r_l = 1$ mm, $r_s = 1.9$ mm, $t_{pm} = 0.1$ mm, $w_l = 14$, $w_s = 12$, $\lambda = 10$, $\gamma = 0$ (color online)

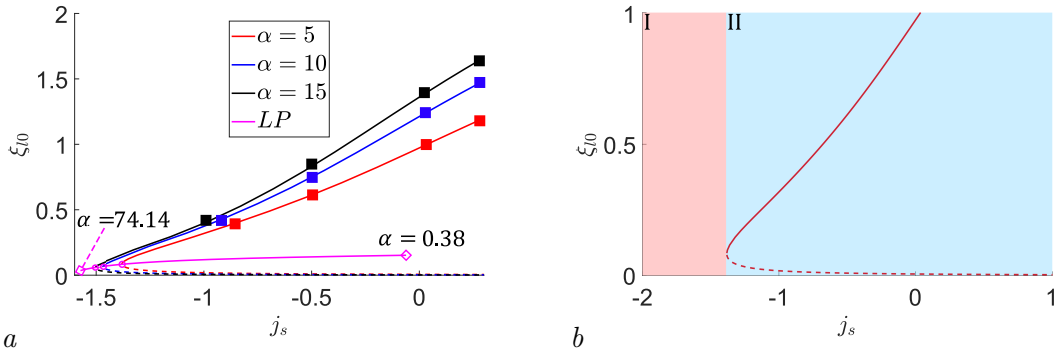

Fig. 5. *a* — Dependence of the average position of RB ξ_{l0} on the parameter j_s at $\alpha = 5, 10, 15$ (red, blue, black lines, respectively); the pink line (LP) indicates the zone of separation of stable (solid lines) and unstable (dashed lines) branches when varying the parameter $\alpha = [0.38; 74.14]$; *b* — depiction of characteristic zones of existence and nonexistence of equilibrium positions at α=5, $\varepsilon = 0.001$, $r_l = 1$ mm, $r_s = 1.9$ mm, $t_{pm} = 0.1$ mm, $w_l = 14$, $w_s = 12$, $\lambda = 10$, $\gamma = 0$ (color online)

minimum magnitude of the current amplitude of the levitation coil I_l) and the corresponding «critical» values of the parameter $\xi_{l0} = \xi_{crit}$, indicating the case of fusion (with subsequent disappearance) of equilibrium states such as «saddle» and «center». As the parameter j_s increases, the value of α_{crit} decreases, and ξ_{crit} increases. The boundary separating the zones of stable and unstable equilibrium branches is represented by a pink line (LP). Pink diamonds indicate the boundary values of the variation of the parameter j_s in the range $[-1; 1]$.

Fig. 5, *a*, *b* shows the dependence of the average position of RB ξ_{l0} on the parameter j_s, which denotes the ratio of the amplitudes of the currents of the levitating and stabilizing coils for different values of the parameter α. With an increase in the amplitude of the stabilizing current, which is antiphase to the current of the levitation coil, the equilibrium position disappears. This is explained by the fact that with an increase in the amplitude of the current of the stabilizing coil, the stabilizing and levitation coils compensate for the magnetic flux through the RB, which leads to a decrease in the induced current, which leads to the disappearance of the average position of the RB. This in turn causes the RB to be attracted to the coils. The dividing line of stable/unstable equilibrium positions is represented when the parameter α varies in the range of $[0.38; 74.14]$.

Fig. 6, *a*, *b* shows the dependence of the levitation height ξ_{l0} on the parameter γ, which denotes the phase difference between the currents i_l, i_s and i_{pm}. It can be seen that ξ_{l0} decreases and as it approaches the «critical» value of $\gamma = \gamma_{crit}$, the levitation regime disappears. This follows from the fact that when the phase difference between the currents i_l, i_s and i_{pm} increases to the value γ_{crit} they can begin to attract, which leads to a malfunction of the device. At $j_s = 1$, that is, if in phase currents are applied to the levitating and stabilizing coils, it can be seen that at $\gamma_{crit} \approx \pi/2$ levitation is not observed.

Fig. 4–6 shows that the «saddle–center» bifurcation corresponds to the boundary value of the variable parameter and defines the region of parameters at which the equilibrium position RB exists. A further stage of the investigation of the bifurcation, which corresponds to one of the pairs of the parameter set $(\alpha^*, \gamma^*, j_s^*)$, consists in continuing consideration of the equilibrium position ξ_{crit} according to one of the active parameters (α, γ or j_s) [50]. To determine the area of existence of the equilibrium position on the planes of the parameters (α, j_s), (γ, j_s), (α, γ) let us carry out the continuation by the parameter of the bifurcation point. The point of confluence of stable and unstable equilibria is chosen for continuation. It is this point that continues above the studied planes and gives the boundary of the area of existence of the average position of the RB. Fig. 7, *a* shows the continuation of the bifurcation point (pink line), Fig. 7, *b–d* denote the zones of absence (I) and presence of two equilibrium states (II) in the parameter space of the system under study.

Fig. 8, *a–d* shows the stability regions (gray area) of the middle position of RB ξ_{l0} according to (15) (black lines), (24) (red lines) at $\gamma = 0.2$, $\lambda = 0.4$. The blue crosses indicate the results of direct integration of system (1).

Fig. 8 shows the stability regions of the middle position of RB.

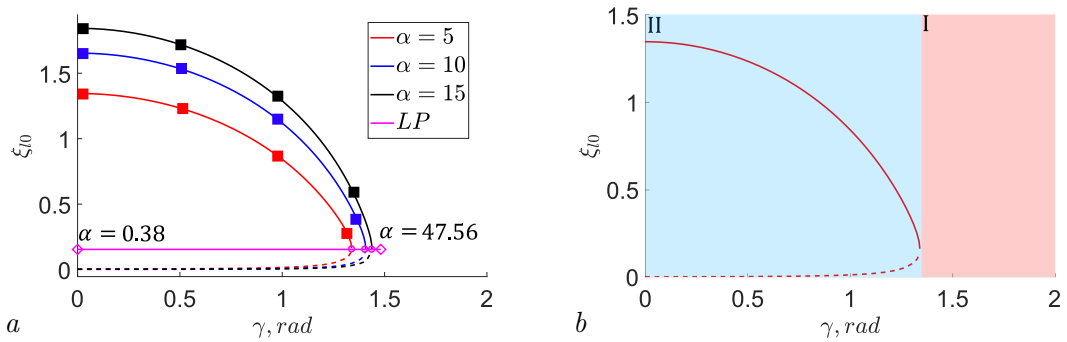

Fig. 6. *a* — Dependence of the average position of RB ξ_{l0} on the parameter γ at $\alpha = 5, 10, 15$ (red, blue, black lines, respectively); the pink line (LP) indicates the zone of separation of stable (solid lines) and unstable (dashed lines) branches when varying the parameter $\alpha = [0.38; 47.56]$; *b* — depiction of characteristic zones of existence and nonexistence of equilibrium positions at $\alpha = 5$, $\varepsilon = 0.001$, $r_l = 1$ mm, $r_s = 1.9$ mm, $t_{pm} = 0.1$ mm, $w_l = 14$, $w_s = 12$, $\lambda = 10$, $j_s = 0$ (color online)

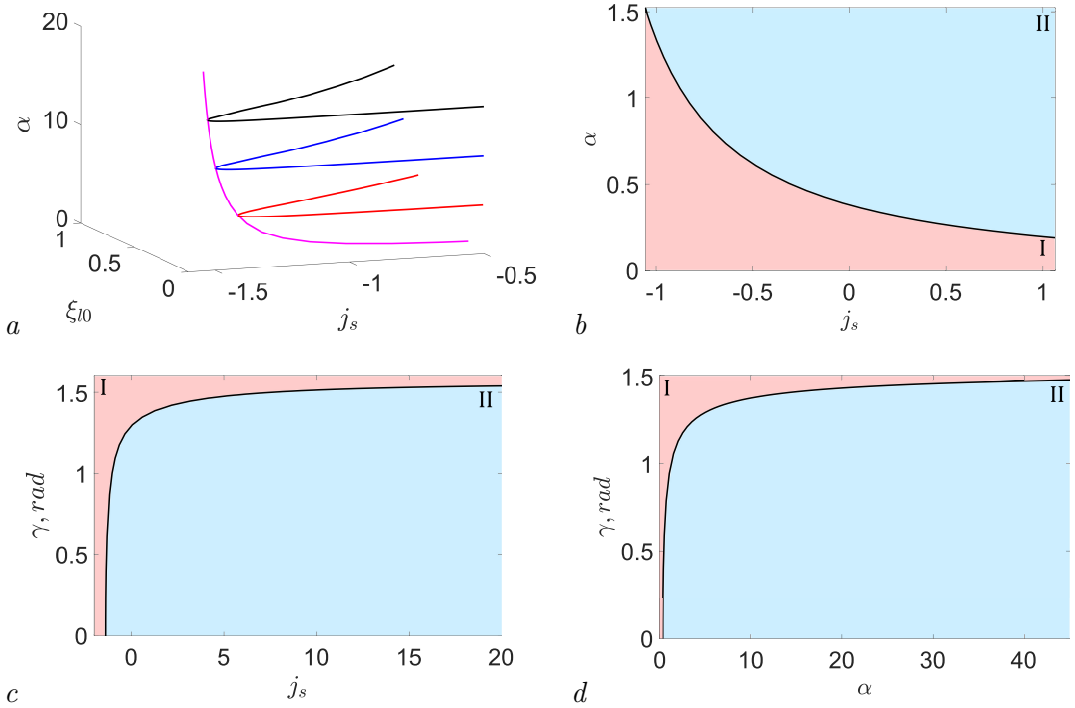

Fig. 7. *a* — Dependence of ξ_{l0} at the saddle-center bifurcation point on parameters α, j_s (pink line); red, blue, black lines — manifold of solutions of ξ_{l0} at varying parameters α, j_s respectively; *b*–*d* — image of zones in the parameter space of the system corresponding to the conditions of the absence and presence of equilibrium states (color online)

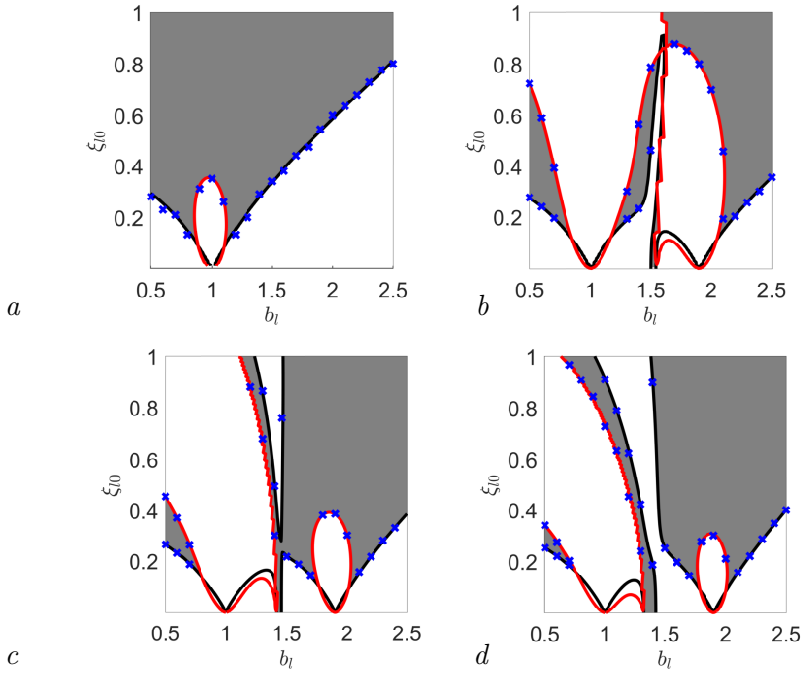

Fig. 8. Evolution of the stability region (gray areas) of the average position of RB ξ_{l0} at: a — $j_s = 0$, b — $j_s = -0.5$, c — $j_s = -0.75$, d — $j_s = -1$, $r_l = 1$ mm, $r_s = 1.9$ mm, $t_{pm} = 0.1$ mm, $w_l = 14$, $w_s = 12$, λ=0.4, γ=0.2, $b_s = \frac{r_l}{r_s} b_l$ according to the formulas (15) (black lines), (24) (red lines); blue crosses — results of direct integration of the system (1) (color online)

Fig. 9, *a*–*c* shows graphs comparing RB oscillations in the case of numerical calculation for various system parameters (ξ_{l0}, b_l), corresponding to the cases: *a* — stable oscillations (gray area in Fig. 8), *b* — unstable oscillations based on a violation of condition (15), *c* — unstable oscillations under the assumption of violation of condition (24).

Fig. 9, *a*–*c* shows that if all inequalities are met in (15), (24) RB oscillations are steady state; if at least one of the inequalities (15), (24) RB movements are divergent.

Fig. 10 shows the dependence of the RB levitation height on time T_0, obtained as a result of numerical calculation in violation of condition (24) in the range $T_0 = [1200; 1250]$. The black line (1) indicates the numerical solution, and the red line (2) indicates the analytical estimate of the drift of the average position of $\sin\sqrt{2b}\varepsilon\tau$, corresponding to expression (25).

As a numerical example, let us estimate the natural frequency and stiffness of an RB made in the form of a thin ring. The physical parameters taken from [51] and accepted for analytical evaluation are shown in Table 2. Here ρ, ρ_{el} are the density and electrical resistivity of the RB material.

Table 2. Physical and geometric parameters of the suspension

Parameter	r_l	r_s	r_{pm}	t_{pm}
Value	1000 μm	1900 μm	1600 μm	25 μm
Parameter	w_l	w_s	ρ	ρ_{el}
Value	20	12	2700 kg/m^3	0.026 μΩ m
Parameter	ω	I_l	I_s	$\hat{m}$
Value	12 MHz	0.11 A	−0.106 A	5.4×10^{-7} kg
Parameter	R_{pm}	g	μ_0	L_{pm}
Value	0.42 ohm	9.8 m/s^2	$4\pi \times 10^{-7}$ H/m	10.14 nH

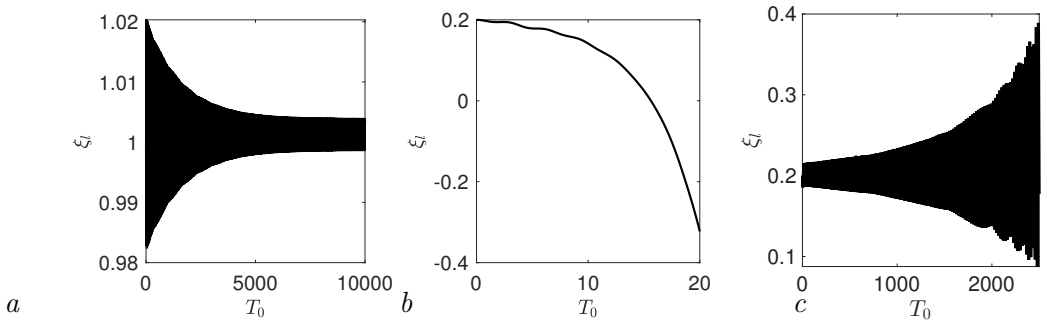

Fig. 9. Graphs of dependence of dimensionless RB displacement on dimensionless time T_0 in the case of direct numerical calculation for: a — $(b_l, \xi_{l0}) = (1, 1)$, b — $(2, 0.2)$, c — $(1, 0.2)$; $j_s = 0$, $r_l = 1$ mm, $r_s = 1.9$ mm, $t_{pm} = 0.1$ mm, $w_l = 14$, $w_s = 12$, $\lambda = 0.4$, $\gamma = 0.2$

In [35] , we analytically obtained an estimate for the dimensionless natural frequency ω_l:

$$\hat{\omega}_l = \varepsilon \sqrt{-\frac{m_l^2 + m_0 m_{ll}}{m_0 m_l}}, \tag{27}$$

from where the dimensional natural frequency ω_l and stiffness c_l are calculated as

$$\omega_l = \omega \hat{\omega}_l, \quad c_l = \hat{m} \omega_l^2. \tag{28}$$

As can be seen from Fig. 10, violation of condition (24) leads to a drift of the average position ξ_{l0}, which is superimposed by oscillations with a dimensionless frequency equal to two. Fig. 11 shows the dependence of the stiffness of the system c_l from the height of levitation RB l (25).

Fig. 11 shows that there are three characteristic zones of dependence of stiffness c_l on the height of levitation l. In the zone of small values of l (red area (I)), the value of c_l takes on negative values (they are not shown in Fig. 11). In the purple region (II), there is a monotonous increase in c_l until reaching a maximum of c_l=c_l^{max}, in the green region (III), with an increase in l, the value of c_l decreases.

Summarizing the above, we emphasize the key features of the RB levitation regime in induction suspension, identified during the study:

Original model (1) has no equilibrium position, only a «fast» oscillatory solution that can be stable or unstable. The oscillation has an «average position», defined as the result of averaging the coordinate on a time scale that is significantly longer than the oscillation period but significantly shorter than other («slow») time scales of the system dynamics.

The dynamics in slow time T_1, described by equation of the conservative nonlinear oscillator (11), may or may not have one or more equilibrium positions ξ_{st}, each of which may be stable or not, depending on the fulfillment of stability condition (15). If the equilibrium position ξ_{st} is stable, then system (11)

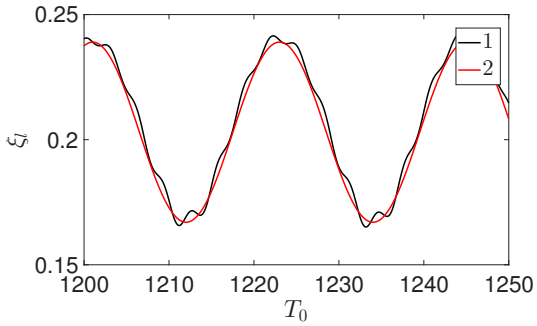

Fig. 10. Graph of the dependence of the dimensionless displacement of the RB on the dimensionless time T_0 in the case of direct numerical calculation for $(b_l, \xi_{l0}) = (1, 0.2)$; $j_s = 0$, $r_l = 1$ mm, $r_s = 1.9$ mm, $t_{pm} = 0.1$ mm, $w_l = 14$, $w_s = 12$, $\lambda = 0.4$, $\gamma = 0.2$. Range $T_0 = [1250 \;\; 1240]$ (color online)

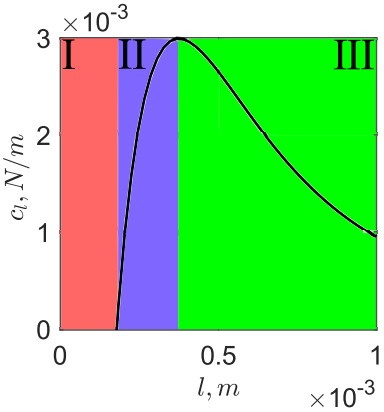

Fig. 11. Graph of dependence of stiffness c_l of the system on the levitation height l (color online)

has a «slow» oscillatory solution (18) in its vicinity; This oscillatory solution is an approximation of slow motion («drift») the «average position» of the original model.

The amplitude dynamics $A = \sqrt{h(T_2)/b}$ of oscillatory solution (18) in an even slower time T_2 is described by 1st order equation (21) having an equilibrium state of $h = 0$. The stability of this state, in turn, is determined by condition (24). If condition (24) is fulfilled, then the slow oscillations («drift of the average position») fade (the total asymptotic solution is stable), otherwise they increase (the total solution is unstable).

Conclusion

In this paper, an analytical model of one-dimensional nonlinear oscillations of a sensitive element of an electromagnetic suspension made in the form of a thin ring made of a conductive material is constructed. An approximate solution to the dynamics issue has been found using asymptotic methods of nonlinear mechanics. Assuming a slow evolution of the average position of the RB, the conditions for the occurrence and parameters of the drift of a levitating rigid body are determined. The stability of the stationary levitation regime is investigated in a refined asymptotic formulation. It is shown that taking into account the possibility of a slow evolution of the average height of levitation leads to the formulation of a stability condition related to the relationship between the dissipation of mechanical and electrical nature.

References

1. Martynenko YuG. Motion of a Rigid Body in Electric and Magnetic Fields. Moscow: Nauka; 1988. 368 p. (in Russian).
2. Skubov D, Khodzhaev KS. Non-Linear Electromechanics. Berlin: Springer; 2008. 471 p. DOI: 10.1007/978-3-540-44779-5.
3. Han HS, Kim DS. Magnetic Levitation: Maglev Technology and Applications. Dordrecht: Springer; 2016. 247 p. DOI: 10.1007/978-94-017-7524-3.
4. Poletkin K. Levitation Micro-Systems: Applications to Sensors and Actuators. Cham: Springer; 2021. 174 p. DOI: 10.1007/978-3-030-58908-0.
5. Poletkin K. Levitating micro-actuators: A review. Actuators. 2018;7(2):17. DOI: 10.3390/ act7020017.
6. Liu K, Zhang W, Chen W, Li K, Dai F, Cui F, Wu X, Ma G, Xiao Q. The development of micro-gyroscope technology. J. Micromech. Microeng. 2009;19(11):113001. DOI: 10.1088/ 0960-1317/19/11/113001.
7. Shearwood C, Ho KY, Williams CB, Gong H. Development of a levitated micromotor for application as a gyroscope. Sensors and Actuators A: Physical. 2000;83(1–3):85–92. DOI: 10.1016/ S0924-4247(00)00292-2.
8. Poletkin K. Thermal Noise in Levitation Micro-Gyroscopes. In: Levitation Micro-Systems. Microsystems

and Nanosystems. Cham: Springer; 2021. P. 135–154. DOI: 10.1007/978-3-030-58908-0_7.
9. Mustafa MNM. Comprehensive review and analysis of the electromagnetic levitation systems (modeling, controllers, nonlinearity sources). E3S Web of Conferences. 2023;371:04027. DOI: 10.1051/e3sconf/202337104027.
10. Poletkin KV, Lu Z, Moazenzadeh A, Mariappan SG, Korvink JG, Wallrabe U, Badilita V. Energy-aware 3D micro-machined inductive suspensions with polymer magnetic composite core. J. Phys.: Conf. Ser. 2018;1052:012048. DOI: 10.1088/1742-6596/1052/1/012048.
11. Shearwood C, Williams CB, Mellor PH, Chang KY, Woodhead J. Electro-magnetically levitated micro-discs. In: IEE Colloquium on Microengineering Applications in Optoelectronics. London: IET; 1996. P. 6/1–6/3. DOI: 10.1049/ic:19960241.
12. Williams CB, Shearwood C, Mellor PH, Yates RB. Modelling and testing of a frictionless levitated micromotor. Sensors and Actuators A: Physical. 1997;61(1–3):469–473. DOI: 10.1016/S0924-4247(97)80307-X.
13. Shearwood C, Williams CB, Mellor PH, Yates RB, Gibbs MRJ, Mattingley AD. Levitation of a micromachined rotor for application in a rotating gyroscope. Electronics Letters. 1995;31(21): 1845–1846. DOI: 10.1049/el:19951232.
14. Williams CB, Shearwood C, Mellor PH, Mattingley AD, Gibbs MRJ, Yates RB. Initial fabrication of a micro-induction gyroscope. Microelectronic Engineering. 1996;30(1–4): 531–534. DOI: 10.1016/0167-9317(95)00302-9.
15. Wu XS, Chen WY, Zhao XL, Zhang WP. Micromotor with electromagnetically levitated rotor using separated coils. Electronics Letters. 2004;40(16):996-997. DOI: 10.1049/el:20040601.
16. Tsai NC, Huang WM, Chiang CW. Magnetic actuator design for single-axis micro-gyroscopes. Microsyst. Technol. 2009;15:493–503. DOI: 10.1007/s00542-008-0769-y.
17. Luan B, Zhang X, Xu F, Yang G, Jin J, Xu C, Sun F, Oka K. High precision magnetic levitation actuator for micro-EDM. Actuators. 2022;11(12):361. DOI: 10.3390/act11120361.
18. Xiao Q, Wang Y, Dricot S, Kraft M. Design and experiment of an electromagnetic levitation system for a micro mirror. Microsyst. Technol. 2019;25:3119–3128. DOI: 10.1007/s00542-019-04452-w.
19. Poletkin K, Lu Z, Wallrabe U, Korvink J, Badilita V. Stable dynamics of micro-machined inductive contactless suspensions. International Journal of Mechanical Sciences. 2017;131: 753–766. DOI: 10.1016/j.ijmecsci.2017.08.016.
20. Jayawant BV. Electromagnetic suspension and levitation. Reports on Progress in Physics. 1981; 44(4):411–477. DOI: 10.1088/0034-4885/44/4/002.
21. Kim NH, Ge L. Dynamic modeling of electromagnetic suspension system. Journal of Vibration and Control. 2013;19(5):729–741. DOI: 10.1177/107754631243860.
22. Gysen BL, Janssen JL, Paulides JJ, Lomonova EA. Design aspects of an active electromagnetic suspension system for automotive applications. IEEE Transactions on Industry Applications. 2009;45(5):1589–1597. DOI: 10.1109/TIA.2009.2027097.
23. Chu SY, Cui X, Zan X, Avestruz AT. Transfer-power measurement using a non-contact method for fair and accurate metering of wireless power transfer in electric vehicles. IEEE Transactions on Power Electronics. 2021;37(2):1244–1271. DOI: 10.1109/TPEL.2021.3105689.
24. Lohöfer G. High-resolution inductive measurement of electrical resistivity and density of electromagnetically levitated liquid metal droplets. Rev. Sci. Instrum. 2018;89:124709. DOI: 10.1063/1.5065482.
25. Udalov P, Lukin A, Popov I, Skubov D. Analysis of the Equilibrium of a Magnetic Contactless Suspension. In: Pandey AK, Pal P, Nagahanumaiah ZL, editors. Microactuators, Microsensors and Micromechanisms. MAMM 2022. Mechanisms and Machine Science. Cham: Springer; 2022. P. 183–190. DOI: 10.1007/978-3-031-20353-4_14.
26. Mamleyev ER, Lee CH, Korvink JG, Kohl M, Poletkin KV, Badilita V. Experimental study and simulation of pull-in behavior in hybrid levitation microactuator for square-shaped proof masses. Actuators. 2023;12(2):48. DOI: 10.3390/act12020048.
27. Okress EC, Wroughton DM, Comenetz G, Brace PH, Kelly JCR. Electromagnetic levitation of solid and molten metals. J. Appl. Phys. 1952;23(5):545–552. DOI: 10.1063/1.1702249.
28. Poletkin K, Chernomorsky AI, Shearwood C, Wallrabe U. A qualitative analysis of designs of

micromachined electromagnetic inductive contactless suspension. International Journal of Mechanical Sciences. 2014;82:110–121. DOI: 10.1016/j.ijmecsci.2014.03.013.
29. Poletkin KV, Lu Z, Wallrabe U, Korvink JG, Badilita V. A qualitative technique to study stability and dynamics of micro-machined inductive contactless suspensions. In: 2017 19th International Conference on Solid-State Sensors, Actuators and Microsystems (TRANSDUCERS). 2017, Kaohsiung, Taiwan. New York: IEEE; 2017. P. 528–531. DOI: 10.1109/TRANSDUCERS.2017.7994102.
30. Shearwood C, Ho KY, Williams CB, Gong H. Development of a levitated micromotor for application as a gyroscope. Sensors and Actuators A: Physical. 2000;83(1–3):85–92. DOI: 10.1016/ S0924-4247(00)00292-2.
31. Poletkin K, Lu Z, Wallrabe U, Badilita V. Hybrid electromagnetic and electrostatic micromachined suspension with adjustable dynamics. J. Phys.: Conf. Ser. 2015;660:012005. DOI: 10.1088/1742-6596/660/1/012005.
32. Poletkin K, Lu Z, Wallrabe U, Badilita V. A new hybrid micromachined contactless suspension with linear and angular positioning and adjustable dynamics. Journal of Microelectromechanical Systems. 2015;24(5):1248–1250. DOI: 10.1109/JMEMS.2015.2469211.
33. Poletkin KV, Chernomorsky AI, Shearwood C, Wallrabe U. An analytical model of micromachined electromagnetic inductive contactless suspension. In: Proceedings of the ASME International Mechanical Engineering Congress and Exposition. 15–21 November, 2013, San Diego, California, USA. P. V010T11A072. DOI: 10.1115/IMECE2013-66010.
34. Xia D, Yu C, Kong L. A micro dynamically tuned gyroscope with adjustable static capacitance. Sensors. 2013;13(2):2176–2195. DOI: 10.3390/s130202176.
35. Udalov PP, Popov IA, Lukin AV, Shtukin LV, Poletkin KV. Parametric stability of microscale contactless inductive suspension with an electrostatic control loop of stiffness. J. Mach. Manuf. Reliab. 2024;53:25–34. DOI: 10.1134/S1052618824010138.
36. Poletkin K, Lu Z, en Hartogh B, Wallrabe U, Badilita V. Stability and spring constant investigation for micromachined inductivesuspensions: Theoretical analysis vs. experimental results. J. Phys.: Conf. Ser. 2014;557:012133. DOI: 10.1088/1742-6596/557/1/012133.
37. Kalantarov PL, Cejtlin LA. Calculation of Inductors: The Reference Book. L.: Energoatomizdat; 1986. 488 p. (in Russian).
38. Rosa EB, Grover FW. Formulas and Tables for the Calculation of Mutual and Self-inductance. Washington, DC: US Government Printing Office; 1948. Vol. 169. 237 p.
39. Poletkin KV. Calculation of magnetic force and torque between two arbitrarily oriented circular filaments using Kalantarov–Zeitlin's method. International Journal of Mechanical Sciences. 2022;220:107159. DOI: 10.1016/j.ijmecsci.2022.107159.
40. Babic S, Akyel C. Magnetic force between inclined circular loops (Lorentz approach). Progress In Electromagnetics Research B. 2012;38:333–349. DOI: 10.2528/PIERB12011501.
41. Poletkin K, Lu Z, Wallrabe U, Korvink J, Badilita V. Stable dynamics of micro-machined inductive contactless suspensions. International Journal of Mechanical Sciences. 2017;131: 753–766. DOI: 10.1016/j.ijmecsci.2017.08.016.
42. Poletkin K. On the static pull-in of tilting actuation in electromagnetically levitating hybrid micro-actuator: Theory and experiment. Actuators. 2021;10(10):256. DOI: 10.3390/ act10100256.
43. Liu K, Zhang W, Liu W, Chen W, Li K, Cui F, Li S. An innovative micro-diamagnetic levitation system with coils applied in micro-gyroscope. Microsyst. Technol. 2010;16: 431–439. DOI: 10.1007/s00542-009-0935-x.
44. Liu W, Zhang W, Chen W. Simulation analysis and experimental study of the diamagnetically levitated electrostatic micromotor. Journal of Magnetism and Magnetic Materials. 2019;492:165634. DOI: 10.1016/j.jmmm.2019.165634.
45. Poletkin K. Quasi-finite Element Modelling. In: Levitation Micro-Systems: Applications to Sensors and Actuators. Cham: Springer; 2021. P. 45–58. DOI: 10.1007/978-3-030-58908-0_4.
46. Lu Z, Jia F, Korvink J, Wallrabe U, Badilita V. Design optimization of an electromagnetic microlevitation system based on copper wirebonded coils. In: Proceedings of the 2012 Power MEMS. 2–5 December 2012, Atlanta, GA. P. 363–366. DOI: 10.13140/2.1.4460.9284.

47. Skubov DYu, Indeitsev DA, Udalov PP, Popov IA, Lukin AV, Poletkin KV. Nonlinear dynamics of a micromechanical non-contact induction suspension. Mech. Solids. 2023;58(6): 2011–2023. DOI: 10.3103/S0025654423600307.
48. Nayfeh AH. Perturbation Methods. New York: John Wiley; 2008. 425 p.
49. Gatzke E. Introduction to MATLAB. In: Introduction to Modeling and Numerical Methods for Biomedical and Chemical Engineers. Cham: Springer; 2022. P. 99–121. DOI: 10.1007/978-3-030-76449-4_6.
50. Dhooge A, Govaerts W, Kuznetsov YA, Meijer HGE, Sautois B. New features of the software MatCont for bifurcation analysis of dynamical systems. Mathematical and Computer Modelling of Dynamical Systems. 2008;14(2):147–175. DOI: 10.1080/13873950701742754.
51. Lu Z, Poletkin K, den Hartogh B, Wallrabe U, Badilita V. 3D micro-machined inductive contactless suspension: Testing and modeling. Sensors and Actuators A: Physical. 2014;220: 134–143. DOI: 10.1016/j.sna.2014.09.017.